



This is the accepted manuscript made available via CHORUS, the article has been published as:

## Magnetic domain wall propagation under ferroelectric control

E. Mikheev, I. Stolichnov, E. De Ranieri, J. Wunderlich, H. J. Trodahl, A. W. Rushforth, S. W. E. Riester, R. P. Campion, K. W. Edmonds, B. L. Gallagher, and N. Setter

Phys. Rev. B **86**, 235130 — Published 19 December 2012

DOI: [10.1103/PhysRevB.86.235130](https://doi.org/10.1103/PhysRevB.86.235130)

# Magnetic Domain Wall Propagation under Ferroelectric Control

By *E. Mikheev*<sup>1</sup>, *I. Stolichnov*<sup>1</sup>, *E. De Ranieri*<sup>2</sup>, *J. Wunderlich*<sup>2</sup>, *H. J. Trodahl*<sup>3</sup>, *A. W. Rushforth*<sup>4</sup>, *S. W. E. Riester*<sup>1</sup>, *R. P. Champion*<sup>4</sup>, *K. W. Edmonds*<sup>4</sup>, *B. L. Gallagher*<sup>4</sup>, *N. Setter*<sup>1</sup>.

<sup>1</sup>Ceramics Laboratory, EPFL-Swiss Federal Institute of Technology, Lausanne 1015, Switzerland

<sup>2</sup>Hitachi Cambridge Laboratory, JJ Thomson Avenue, Cambridge, CB3 0HE, UK

<sup>3</sup>MacDiarmid Institute for Advanced Materials and Nanotechnology, Victoria University, Wellington, New Zealand

<sup>4</sup>School of Physics and Astronomy, University of Nottingham, Nottingham NG7 2RD, UK

## *Abstract*

Control of magnetic domain walls (DWs) and their propagation is among the most promising development directions for future information-storage devices. The well-established tools for such manipulation are the spin-torque transfer from electrical currents and strain. The focus of this work is an alternative concept based on the non-volatile ferroelectric field effect on DWs in a ferromagnet with carrier-mediated exchange coupling. The integrated ferromagnet/ferroelectric structure yields two superimposed ferroic patterns strongly coupled by electric field. Using this coupling we demonstrate an easy to form, stable, non-destructive, and electrically re-writable switch on magnetic domain wall propagation.

The search for strongly-coupled magnetoelectric multiferroics is driven by both the interesting fundamentals and the potential for exploitation in novel spintronic-type devices<sup>1-3</sup>. Of particular practical interest from the device point of view are hetero-layered systems with an extrinsic charge-mediated coupling, featuring a ferromagnet with carrier concentration-sensitive properties and a ferroelectric as a source of a non-volatile field effect. Prominent examples of such combinations are lanthanum manganites with oxide ferroelectrics<sup>4,5</sup> and dilute magnetic semiconductors (DMS) with polymer ferroelectrics<sup>6</sup>. Closely related is the large body of work using various dielectrics in place of ferroelectrics for volatile control of ferromagnetism in field effect transistor (FET)-like structures<sup>7-11</sup>.

Efforts to date have focused largely on controlling the hysteresis in the ferromagnetic phase, e.g. switching between paramagnetic and ferromagnetic orders<sup>7,9,10,12</sup>, control of magnetization magnitude<sup>4,9,12</sup> or its coercive field<sup>6,12</sup>. Generally, in the case of charge-driven coupling, the origin of these effects can ultimately be traced to a modulation of the ferromagnetic transition temperature ( $T_C$ ). It largely tends to be a relatively weak effect limited to a shift of 10-20 K (as in<sup>4,9</sup>) or less between the two device states.

A promising, more subtle approach is to switch some further details of the ferromagnetic order. For instance, there have been encouraging results in the attempts to induce magnetization rotation by changing the easy magnetic axis orientation by field effect<sup>13,14</sup> or strain<sup>15-17</sup>. Possibility of strain-mediated control of magnetic domain pattern and DW motion in two-component metal/ferroelectric systems has been demonstrated<sup>18-</sup>

<sup>20</sup>. A volatile electrostatic control of domain wall velocity via a gate dielectric has been achieved in ultrathin cobalt<sup>21</sup>. Such phenomena are also under intense investigation in single-component ferromagnetic systems, such as nanowires of transition metals and dilute magnetic semiconductors, where strain<sup>22–24</sup> and spin-transfer torque<sup>25,26</sup> can be used as manipulation tools. Such control of domain propagation under spin-polarized electrical current pulses is the cornerstone of the racetrack memory concept, which uses DW sequences as memory bits<sup>27–29</sup>.

In this paper, we demonstrate electrostatic control of magnetic domains in a hetero-layered DMS/ferroelectric system. Its essential functionality is the possibility to electrically write a reversible and non-volatile DW propagation switch. This control is unambiguously observed by the strong footprints of DWs in magnetotransport arising from the Extraordinary Hall Effect (EHE). Moreover, we use the magneto-optical Kerr Effect (MOKE) as a direct demonstration, imaging ferromagnetic domain patterns that are controlled by the ferroelectric polarization.

We first present magnetotransport measurements based on the structure illustrated in Fig. 1a, a ferroelectric-gate FET using a DMS (Mn-doped GaAs) channel<sup>30</sup>. The channel was codoped with phosphorus in order to produce tensile strain in the epitaxial film and thus rotate the easy axis from the common in-plane (IP) to the out-of-plane (OOP) direction<sup>31–33</sup>. As will be seen below, this feature is essential, as it introduces in our system magnetic domain walls<sup>31,34</sup> between the two OOP directions of magnetization  $M$ . The ferroelectric gate was formed by the ferroelectric polymer P(VDF-TrFE), whose polarization hysteresis loop is seen in Fig 1b. Here we will show transport data for channels under the remnant polarizations, marked by empty circles. The electric field

from the remnant polarization controls the carrier density in the channel, forming stable depletion and accumulation of the holes in the valence band of the channel<sup>35</sup>. The carrier density controls in turn the Mn-Mn exchange, and thus  $T_C$  and the properties of the ferromagnetic state of the DMS channel<sup>36,37</sup>.

The EHE is proportional to the perpendicular component of the magnetization vector, yielding the most direct transport signature in the Hall resistance  $R_{XY}$  of the (Ga,Mn)(As,P) channel. The response to a magnetic field  $B$  applied along the OOP direction was found to be clearly hysteretic below  $T_C$  (Fig. 1c). The gate-induced collapse of this hysteresis near  $T_C$  (28 K) and the modulation of its coercivity are consistent with its downward (upward) shift in the depletion (accumulation) state of the ferroelectric gate, as reported previously<sup>6,38</sup>.

The data in Fig. 1c were obtained on an as-grown channel, in which  $T_C$  is suppressed due to carrier compensation by interstitial Mn defects<sup>36</sup>. We have demonstrated previously that  $T_C$  can be recovered under a low-temperature annealing regime<sup>38</sup> by removing these interstitial Mn ions from the DMS layer<sup>39</sup>. In the present report we have focused on the behavior of such structures in which the channel has been annealed at 130°C for 5 and for 10 hours. The recovered high  $T_C$  following the annealing process<sup>30</sup> is a direct result of an increase in the carrier (hole) concentration in annealed films, as illustrated by the conductivity data of Fig. 1d. The gate modulation under depletion/accumulation is of course limited in the more heavily doped (annealed) films, but the detection of DW signatures in magnetotransport is greatly simplified.

For an OOP easy axis the investigation of DW motion is conveniently accomplished by monitoring the Hall ( $R_{XY}$ ) and longitudinal ( $R_{XX}$ ) resistances in the

geometry shown in Fig. 2a, with the applied field  $B$  now in-plane and parallel to the current  $I$  ( $B \parallel I$ ). The essential advantage of this geometry is that the magnetization reversal process is driven by the very small OOP field component  $B_z$ , due to the experimental misalignment between  $B$  and the Hall bar plane (Fig. 2b). The reversal process is then drawn out over a larger applied field range to the point where DW propagation can be examined.

The full sequence of magnetization rotations is readily observed in the measurement of  $R_{XY}$  (Fig. 2c), which follows the EHE and thus provides a direct measure of the OOP component of  $M$ <sup>40,41</sup>. Referring to Fig. 2c, for a sweep from positive to negative field: at step (I)  $B$  is positive and strong enough to force  $M$  along the hard axis (IP), resulting in an IP monodomain state. (II) As the field is reduced,  $M$  rotates towards its easy axis (OOP). Importantly,  $M$  is aligned in one direction by the vertical field component  $B_z$ . (III) As the signs of  $B$  and  $B_z$  are reversed, there is a gradual reversal of  $M$  towards the opposite OOP direction. (IV) At high negative  $B$ ,  $M$  is once again forced into an IP monodomain state along the IP direction. The following reverse field sweep mirrors these processes.

The presence of domain-walls is clearly seen in the longitudinal resistance  $R_{XX}$ , which displays asymmetric spikes (Fig. 2d) upon magnetization reversal. This signature originates from circulating components of the electrical currents passing through domain walls, leading to the admixture of EHE into the measurement of  $R_{XX}$ <sup>40–43</sup>. The spikes thus occur only when there are domain boundaries in the Hall bar, i.e. when the bar is in a multi-domain state.

Of particular interest is the step (III) in the magnetization rotation sequence, where the coercive point of  $R_{XY}$  signals the absence of a preferential orientation of  $M$ . It occurs at the same point in field as the asymmetric spike in  $R_{XX}$  and can be interpreted as the point of maximum DW density<sup>44</sup>. The coincidence of these two signatures in our samples is consistently observed over a wide range of temperature and offset angles<sup>30</sup>.

The heavily annealed (Ga,Mn)(As,P) channel of Fig. 2c and d shows unmistakable signatures of the progressive switch between two single-domain states accompanied by domain wall propagation. However, the ferroelectric control in this channel was limited due to its high hole concentration. In contrast, the much lower hole concentration (and higher resistance) in samples without post-growth annealing allows for a much higher degree of control (Fig. 2e and f). This functionality is illustrated by the Hall resistance with  $B \parallel I$  in Fig. 2e. At a temperature of 18 K the separation between the two reversals of  $M$ , signaled by the Hall resistance crossing through zero, is obvious for both the accumulation and depletion polarization. By 24 K the depletion state shows no opening, confirming that  $T_C$  has been exceeded, but in accumulation the hysteretic opening remains even at 28 K. These observations are summarized in Fig. 2f, which shows this opening plotted vs temperature. The 20% modulation of  $T_C$  is the largest we have achieved to date. However, the asymmetric peaks in  $R_{XX}$  signaling DW propagation are masked in this channel by its very high electrical resistance.

We turn finally to the intermediate hole concentration film achieved with a five-hour anneal (right-hand section of Fig. 2). At 41 K (Fig. 2g), the accumulation state yields a clear hysteresis in the Hall ( $R_{XY}$ ) resistance, whose coercive point is coincident with a spike in the sheet ( $R_{XX}$ ) resistance. Both these signatures of magnetization reversal

through DW propagation are absent in the depletion state at this temperature, but are recovered at 38K (upper panel of Fig. 2g). Fig 2f has more detailed data<sup>30</sup> for every 0.5 K between 38 and 44 K with  $R_{XX}$  peak and  $R_{XY}$  crossover fields plotted against temperature. It is clear that the observed effect originates from a  $T_C$  shift of 3.5K (8%). Both the absolute value and the shift of  $T_C$  observed in this experiment correlate very well with the ones signaled by the cusp in the temperature derivative of sheet resistance  $dR_{XX}/dT$  (Fig. 2i, and Supplementary Figure 2<sup>30</sup>). Annealing the device seeks to exploit a trade-off between the improved clarity of the domain reversal signatures and the reduced temperature gap between accumulation and depletion. Nevertheless, this compromise situation clearly demonstrates the non-volatile switching of both studied signatures: coercive point of Hall voltage indicating magnetization switching and longitudinal resistance spike characteristic of DW propagation.

We have confirmed the change of ferromagnetic domain dynamics associated with the ferroelectric field effect using magneto-optical polar Kerr effect (MOKE) microscopy. The transparent nature of the polymer ferroelectric gate offers a valuable benefit of optical access, which allows for direct visualization of the ferromagnetic state switching via the MOKE technique. This experiment was carried out on Hall bars fabricated from the same material in the same processing run as the ones used for the transport measurements presented above. These samples were annealed post-processing for 1h at 130° in order to enhance the measurable MOKE signal.

Prior to placing the samples into the MOKE system the polarization in the polymer ferroelectric was patterned by applying 30V to an atomic force microscope (AFM) tip while scanning a region of 50x50  $\mu\text{m}$ , as sketched in Fig. 3a. The stability and uniformity



of the polarization within the poled area have been confirmed by mapping the amplitude and phase of the local piezoelectric response<sup>45</sup> performed 24h after poling (fig. 3b and c). During the MOKE experiments, a perpendicular magnetic field of a few mT was first applied to the sample in order to induce a fully switched monodomain state. Then the magnetic field direction was reversed and the field was swept by small steps of 0.02 mT to the opposite polarity. After each step a MOKE image has been collected from the area of 75x100  $\mu\text{m}$  covering the border between the poled and non-poled regions and subtracted from a reference picture in the saturated state.

The resulting differential pictures in Fig. 3(d, e) and movie 3d in supplementary material clearly show the influence of ferroelectric polarization on the ferromagnetic DW propagation. At 31K (3-4K below  $T_C$ ) the DMS area under the region of the ferroelectric poled by the AFM tip in depletion switches at lower fields compared to the surrounding (unpoled) regions, with multiple nuclei of opposite domains. This observation is fully consistent with a lower  $T_C$  and coercive field in depletion state, as expected from the magnetotransport data of Fig. 2. The boundary of the poled ferroelectric area clearly projects on the MOKE images, directly showing that the propagation of the magnetic domains is impeded by this boundary. Similar measurements repeated at 25K (about 10K below  $T_C$ ) demonstrate similar behavior with multiple nucleation sites clearly seen at the initial phase of the switching process. The occurrence of this transient multidomain configuration is in agreement with the appearance of the asymmetric spikes in the longitudinal magnetotransport.

The patterning of the ferroelectric gate was also carried out with an alternative technique, using a standard top gate electrode for application of a 30V bias to the

ferroelectric gate. After poling the gold gate electrode was chemically removed by wet etching in order to optically access the channel (Fig. 3f). Ferroelectric patterns obtained with this method induce similar changes in the ferromagnetic domain dynamics. Poling in the accumulation (depletion) state impedes (facilitates) the ferromagnetic switching as shown in the series of images in figures 3 (g, h) and movie 3g in supplementary material. In both cases the boundary of poled/unpoled regions of the polymer gate projects on the magnetic channel as a sharp border between two oppositely magnetized domains. This border remains stable resisting the magnetic domain propagation while the external magnetic field is increased by 0.3-0.35 mT, then a monodomain state gradually sets on. These experiments validate results obtained on the AFM-poled area by showing the same behavior on the areas poled with the conventional electrodes. These data indicate that the change of magnetic properties is a result of the ferroelectric gate effect rather than any alternative mechanism based on magnetic material modification due to the very high electric field in the vicinity of the AFM tip.

The ensemble of Fig. 3 confirms a strong coupling between the superimposed ferroelectric and ferromagnetic domain patterns. By selectively patterning the ferroelectric polarization, one can locally increase or decrease the field threshold for magnetic domain reversal. This can be used to control the direction of DW propagation or to trigger domain nucleation at preferential sites.

Using this gate effect as a tool for manipulation of magnetic domains and DWs is attractive because of its non-volatile and re-writable nature. This makes it an intriguing complement to the existing concepts of magnetic DW logic using electrical currents to induce their propagation<sup>27,28</sup>. A number of functionalities of interest for such logic can be

enabled by the addition of the non-volatile gate, such as definition of racetrack geometries, particular pinning sites for DWs and voltage switches for closing/opening racetracks for DWs. Moreover, ferroelectric polarization in P(VDF-TrFE) lends itself readily to the definition of complex patterns, including the possibility of lateral downscaling with resolution down to several tens of nm<sup>46</sup>. Therefore, while beyond the scope of this work, the DMS/P(VDF-TrFE) system can provide a unique opportunity to study DW dynamics at the nanoscale without the use of lithography.

### Acknowledgments

Co-authors from EPFL acknowledge support from the Swiss National Science Foundation: Project 200020\_132724. EU is acknowledged for financial support through the projects ERC- 268058 MOBILE-W, COST-0904 and 214499 – NAMASTE. AWR acknowledges support from a UK EPSRC Career Acceleration Fellowship (EP/H003487/1).

### References and Notes

- <sup>1</sup> W. Eerenstein, N.D. Mathur, and J.F. Scott, *Nature* **442**, 759 (2006).
- <sup>2</sup> C.A.F. Vaz, J. Hoffman, C.H. Ahn, and R. Ramesh, *Advanced Materials* **22**, 2900 (2010).
- <sup>3</sup> C.A.F. Vaz, *Journal of Physics: Condensed Matter* **24**, 333201 (2012).
- <sup>4</sup> H.J.A. Molegraaf, J. Hoffman, C.A.F. Vaz, S. Gariglio, D. van der Marel, C.H. Ahn, and J.-M. Triscone, *Advanced Materials* **21**, 3470 (2009).
- <sup>5</sup> C.A.F. Vaz, J. Hoffman, Y. Segal, J.W. Reiner, R.D. Grober, Z. Zhang, C.H. Ahn, and F.J. Walker, *Physical Review Letters* **104**, 127202 (2010).
- <sup>6</sup> I. Stolichnov, S.W.E. Rieder, H.J. Trodahl, N. Setter, A.W. Rushforth, K.W. Edmonds, R.P. Campion, C.T. Foxon, B.L. Gallagher, and T. Jungwirth, *Nature Materials* **7**, 464 (2008).
- <sup>7</sup> H. Ohno, D. Chiba, F. Matsukura, T. Omiya, E. Abe, T. Dietl, Y. Ohno, and K. Ohtani, *Nature* **408**, 944 (2000).
- <sup>8</sup> M. Weisheit, S. Fähler, A. Marty, Y. Souche, C. Poinsignon, and D. Givord, *Science* **315**, 349 (2007).
- <sup>9</sup> M. Sawicki, D. Chiba, A. Korbecka, Y. Nishitani, J.A. Majewski, F. Matsukura, T. Dietl, and H. Ohno, *Nature Physics* **6**, 22 (2009).

- <sup>10</sup> Y. Yamada, K. Ueno, T. Fukumura, H.T. Yuan, H. Shimotani, Y. Iwasa, L. Gu, S. Tsukimoto, Y. Ikuhara, and M. Kawasaki, *Science* **332**, 1065 (2011).
- <sup>11</sup> D. Chiba, S. Fukami, K. Shimamura, N. Ishiwata, K. Kobayashi, and T. Ono, *Nature Materials* **10**, 853 (2011).
- <sup>12</sup> D. Chiba, M. Yamanouchi, F. Matsukura, and H. Ohno, *Science* **301**, 943 (2003).
- <sup>13</sup> D. Chiba, M. Sawicki, Y. Nishitani, Y. Nakatani, F. Matsukura, and H. Ohno, *Nature* **455**, 515 (2008).
- <sup>14</sup> T. Maruyama, Y. Shiota, T. Nozaki, K. Ohta, N. Toda, M. Mizuguchi, A.A. Tulapurkar, T. Shinjo, M. Shiraishi, S. Mizukami, Y. Ando, and Y. Suzuki, *Nature Nanotechnology* **4**, 158 (2009).
- <sup>15</sup> M. Overby, A. Chernyshov, L.P. Rokhinson, X. Liu, and J.K. Furdyna, *Applied Physics Letters* **92**, 192501 (2008).
- <sup>16</sup> A.W. Rushforth, E. De Ranieri, J. Zemen, J. Wunderlich, K.W. Edmonds, C.S. King, E. Ahmad, R.P. Campion, C.T. Foxon, B.L. Gallagher, K. Výborný, J. Kučera, and T. Jungwirth, *Physical Review B* **78**, 085314 (2008).
- <sup>17</sup> M. Weiler, A. Brandlmaier, S. Geprägs, M. Althammer, M. Opel, C. Bihler, H. Huebl, M.S. Brandt, R. Gross, and S.T.B. Goennenwein, *New Journal of Physics* **11**, 013021 (2009).
- <sup>18</sup> T.H.E. Lahtinen, J.O. Tuomi, and S. van Dijken, *Advanced Materials* **23**, 3187 (2011).
- <sup>19</sup> T.H.E. Lahtinen, K.J. Franke, and S. van Dijken, *Scientific Reports* **2**, 258 (2012).
- <sup>20</sup> D.E. Parkes, S.A. Cavill, A.T. Hindmarch, P. Wadley, F. McGee, C.R. Staddon, K.W. Edmonds, R.P. Campion, B.L. Gallagher, and A.W. Rushforth, *Applied Physics Letters* **101**, 072402 (2012).
- <sup>21</sup> D. Chiba, M. Kawaguchi, S. Fukami, N. Ishiwata, K. Shimamura, K. Kobayashi, and T. Ono, *Nature Communications* **3**, 888 (2012).
- <sup>22</sup> T.-K. Chung, S. Keller, and G.P. Carman, *Applied Physics Letters* **94**, 132501 (2009).
- <sup>23</sup> T. Brintlinger, S.-H. Lim, K.H. Baloch, P. Alexander, Y. Qi, J. Barry, J. Melngailis, L. Salamanca-Riba, I. Takeuchi, and J. Cumings, *Nano Letters* **10**, 1219 (2010).
- <sup>24</sup> J. Wunderlich, A.C. Irvine, J. Zemen, V. Holý, A.W. Rushforth, E. De Ranieri, U. Rana, K. Výborný, J. Sinova, C.T. Foxon, R.P. Campion, D.A. Williams, B.L. Gallagher, and T. Jungwirth, *Physical Review B* **76**, 054424 (2007).
- <sup>25</sup> M. Yamanouchi, D. Chiba, F. Matsukura, and H. Ohno, *Nature* **428**, 539 (2004).
- <sup>26</sup> M. Hayashi, L. Thomas, R. Moriya, C. Rettner, and S.S.P. Parkin, *Science* **320**, 209 (2008).
- <sup>27</sup> D.A. Allwood, G. Xiong, C.C. Faulkner, D. Atkinson, D. Petit, and R.P. Cowburn, *Science* **309**, 1688 (2005).
- <sup>28</sup> S.S.P. Parkin, M. Hayashi, and L. Thomas, *Science* **320**, 190 (2008).
- <sup>29</sup> G. Catalan, J. Seidel, R. Ramesh, and J. Scott, *Reviews of Modern Physics* **84**, 119 (2012).
- <sup>30</sup> See Supplemental Material at [URL] for device fabrication details, additional transport and magnetotransport data and movies of controlled domain wall propagation as seen by MOKE.
- <sup>31</sup> A. Lemaitre, A. Miard, L. Travers, O. Mauguin, L. Largeau, C. Gourdon, V. Jeudy, M. Tran, and J.-M. George, *Applied Physics Letters* **93**, 021123 (2008).

- <sup>32</sup> A.W. Rushforth, M. Wang, N.R.S. Farley, R.P. Champion, K.W. Edmonds, C.R. Staddon, C.T. Foxon, and B.L. Gallagher, *Journal of Applied Physics* **104**, 073908 (2008).
- <sup>33</sup> A. Casiraghi, A.W. Rushforth, M. Wang, N.R.S. Farley, P. Wadley, J.L. Hall, C.R. Staddon, K.W. Edmonds, R.P. Champion, C.T. Foxon, and B.L. Gallagher, *Applied Physics Letters* **97**, 122504 (2010).
- <sup>34</sup> S. Haghgoo, M. Cubukcu, H. von Bardeleben, L. Thevenard, A. Lemaître, and C. Gourdon, *Physical Review B* **82**, 041301 (2010).
- <sup>35</sup> I. Stolichnov, S.W.E. Riester, E. Mikheev, N. Setter, A.W. Rushforth, K.W. Edmonds, R.P. Champion, C.T. Foxon, B.L. Gallagher, T. Jungwirth, and H.J. Trodahl, *Nanotechnology* **22**, 254004 (2011).
- <sup>36</sup> T. Jungwirth, K. Wang, J. Mašek, K. Edmonds, J. König, J. Sinova, M. Polini, N. Goncharuk, A. MacDonald, M. Sawicki, A. Rushforth, R. Champion, L. Zhao, C. Foxon, and B. Gallagher, *Physical Review B* **72**, 165204 (2005).
- <sup>37</sup> Y. Nishitani, D. Chiba, M. Endo, M. Sawicki, F. Matsukura, T. Dietl, and H. Ohno, *Physical Review B* **81**, 045208 (2010).
- <sup>38</sup> I. Stolichnov, S.W.E. Riester, E. Mikheev, N. Setter, A.W. Rushforth, K.W. Edmonds, R.P. Champion, C.T. Foxon, B.L. Gallagher, T. Jungwirth, and H.J. Trodahl, *Physical Review B* **83**, 115203 (2011).
- <sup>39</sup> K.W. Edmonds, P. Bogusławski, K.Y. Wang, R.P. Champion, S.N. Novikov, N.R.S. Farley, B.L. Gallagher, C.T. Foxon, M. Sawicki, T. Dietl, M. Buongiorno Nardelli, and J. Bernholc, *Physical Review Letters* **92**, 037201 (2004).
- <sup>40</sup> G. Xiang, A. Holleitner, B. Sheu, F. Mendoza, O. Maksimov, M. Stone, P. Schiffer, D. Awschalom, and N. Samarth, *Physical Review B* **71**, 241307 (2005).
- <sup>41</sup> G. Xiang and N. Samarth, *Physical Review B* **76**, 054440 (2007).
- <sup>42</sup> H. Tang and M. Roukes, *Physical Review B* **70**, 205213 (2004).
- <sup>43</sup> X. Cheng, S. Urazhdin, O. Tchernyshyov, C. Chien, V. Nikitenko, A. Shapiro, and R. Shull, *Physical Review Letters* **94**, 017203 (2005).
- <sup>44</sup> It is important to note that both these signatures rely on a small misalignment of the field, for which we have carefully maintained a constant offset ( $\sim 1^\circ$ ) in the present experiment to permit direct comparison between the depletion and accumulation measurements.
- <sup>45</sup> R. Gysel, I. Stolichnov, A.K. Tagantsev, S.W.E. Riester, N. Setter, G.A. Salvatore, D. Bouvet, and A.M. Ionescu, *Applied Physics Letters* **94**, 263507 (2009).
- <sup>46</sup> B.J. Rodriguez, S. Jesse, S. V. Kalinin, J. Kim, S. Ducharme, and V.M. Fridkin, *Applied Physics Letters* **90**, 122904 (2007).

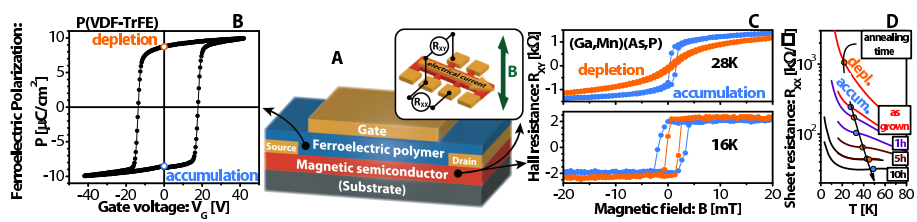


Figure 1

BW11560 26NOV2012

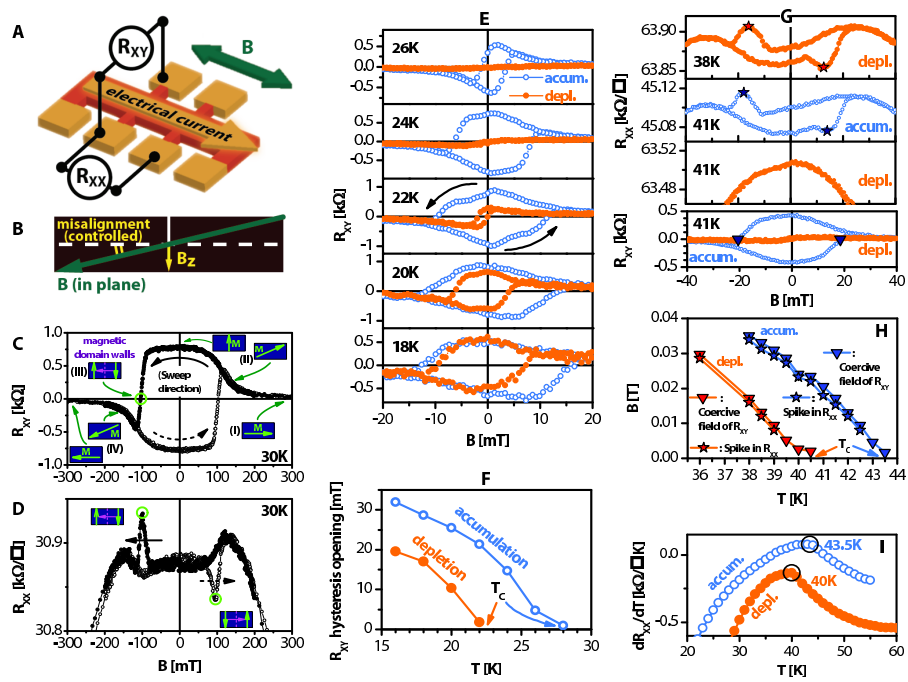


Figure 2

BW11560

26NOV2012

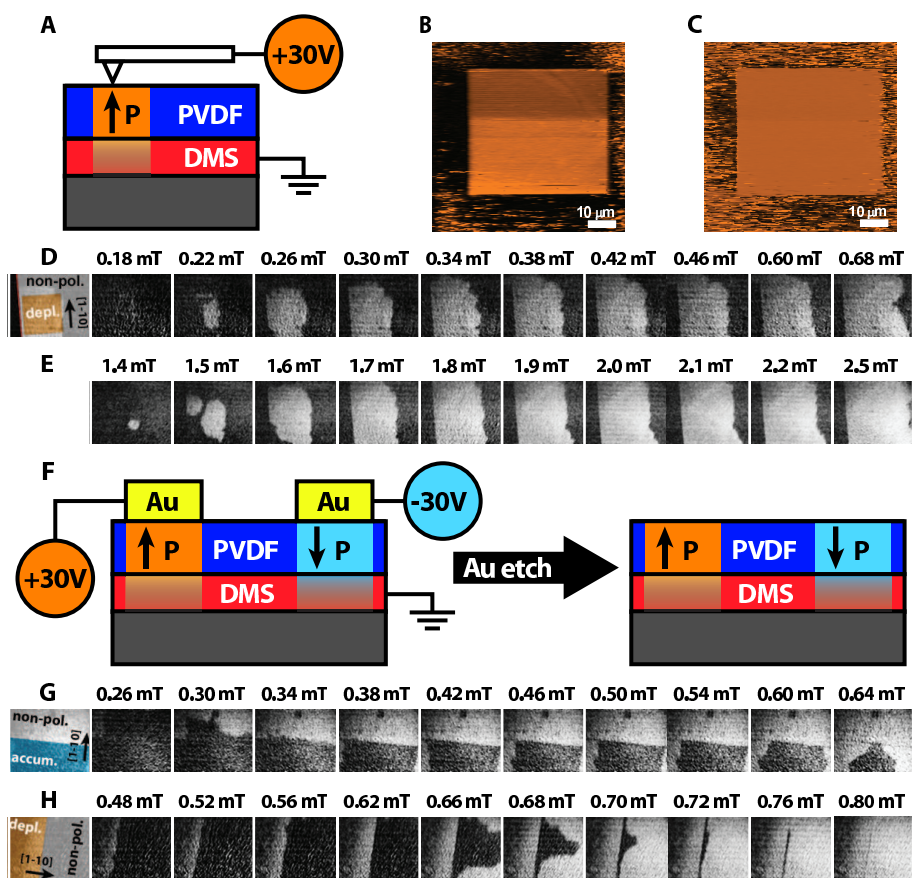


Figure 3

BW11560

26NOV2012